Journal of Chemical and Petroleum Engineering (JChPE)

Print ISSN: 2423-673X Online ISSN: 2423-6721

Neural Network Modeling for Development of High-Pressure Measurement of Carbon Dioxide Solubility in the Aqueous AEEA+Sulfolane

Arman Hasanzadeh, Ahad Ghaemi, Shahrokh Shahhosseini *

1. School of Chemical, Petroleum and Gas Engineering, Iran University of Science and Technology, Tehran, Iran. E-mail: arhas.chemeng@gmail.com
2. School of Chemical, Petroleum and Gas Engineering, Iran University of Science and Technology, Tehran, Iran. E-mail: aghaemi@iust.ac.ir
3. School of Chemical, Petroleum and Gas Engineering, Iran University of Science and Technology, Tehran, Iran. E-mail: shahrokh@iust.ac.ir

ARTICLE INFO

Article History:
Received: 07 July 2022
Revised: 01 June 2023
Accepted: 06 June 2023

Article type: Research

Keywords:
CO_2,
MLP,
RBF,
Modeling,
Solubility

ABSTRACT

Due to increasing concerns about global warming regarding CO_2 release to the atmosphere, various methods are used to capture CO_2, among which chemical absorption via amine mixture solutions is very well developed. A set of 179 data related to CO_2 absorption in a mixture, including a physical absorbent (sulfolane) and a chemical absorption (AEEA) in a wide range of temperature, pressure and solvent concentration is used to develop two Artificial Neural Networks (ANN). In Multi-Layer Perceptron (MLP), the Levenberg-Marquardt method is used to train the network. Most important factors such as regression analysis value (R^2) of 0.99963, Mean Squared Error (MSE) value of 1.22E-05 and Average Absolute Relative Deviation value (%AARD) of 0.2671 factors reveal that the MLP network has a high capability to predict CO_2 loading (α_{CO2}). Also, a Radial Basis Function (RBF) network was developed. RBF network with a spread value of 2.2 and 138 neurons had an outstanding performance and achieved an MSE value of 2.53E-05 along with an R^2 value of 0.99993, 11 seconds, and a %AARD value of 0.1460. According to experimental and predicted data, the neural networks are well trained and are able to predict CO_2 loading precisely in an economic and optimized way.

Introduction

Global warming has become a significant concern due to the increasing release of greenhouse gases into the atmosphere. Since the increase of global mean temperature has a massive effect on the environment, it is vital to mitigate the emissions of such gases. The most significant contributor to global warming is CO2 [1], so it is crucial to find somehow routes to decrease CO2 outpouring.

Researchers have investigated and tested different effective ways to separate CO2 from many mixtures in the last decades. There are three major categories of CO2 capture, pre-combustion, oxy-fuel combustion, and post-combustion [2]. The most mature and most used technologies are

* Corresponding Authors: S. Shahhosseini (E-mail address: shahrokh@iust.ac.ir)

Journal of Chemical and Petroleum Engineering, 2023, 57(2): 179- 202.
Publisher: University of Tehran, College of Engineering *DOI: 10.22059/jchpe.2023.345296.1397*

developed under the post-combustion category, mainly of exhaust gas released from fossil fuel power plants [3].

CO2 capture by chemical absorption is now a rising method using absorbents like amines, ionic liquids, inorganic compounds, and their blends [4]. Due to the variant molecular structure of Amines, there are some advantages and disadvantages for primary, secondary, tertiary, and hindered amines [2]. While blending them, it is a matter of finding the best and optimal ratio of concentrations [5].

The selection of a suitable compound depends on the flue gas's composition, temperature, and pressure. Corrosion rate, equipment size, and energy penalty during regeneration of solvents are the most critical obstacles of chemical absorption, which will be fixed by modifying the process and the solvent(s). MEA is the most common alkanolamine solvent used to absorb CO2 [2]. There are other types of alkanolamines, such as DEA (a secondary amine) and MDEA (a tertiary amine), that also have disadvantages when used as a single solvent. Researchers have suggested using blends of alkanolamines like Methanol+MEA, NMP+DEG, Piperazine+MDEA, etc., that have the favorable properties of every single solvent in a mixture of solvents. These solvents could perform better due to higher solubility and diffusivity [6, 7].

Generally, there are three generations of CO2 solvents. The first generation solvents investigated in CCS were related to conventional gas scrubbing processes. Amines with suitable selectivity to absorb CO2 belonged to alkanolamines [8]. Triethanolamine (TEA) as a tertiary amine is the first commercial solvent used for gas purification, and afterward MEA and DEA were then utilized afterward. MDEA (tertiary), DGA (primary), and DIPA (secondary) were also used [9]. Typically, CO2-amine reactivity related to the solvents, as mentioned earlier, has shown a linear behavior from a kinetic and regeneration energy point of view due to amines' chemical structure. Primary and secondary amines produce carbamate ions by reacting with CO2, which increases the regeneration energy of solvents [10]. Due to carbamate formation, primary and secondary amines have a higher absorption rate than tertiary amines. Solvents that form carbamate have a higher reaction rate, which reduces equipment size. So there should be a trade-off between a suitable absorption rate and a low regeneration penalty [11].

Second generation solvents are functionalized solvents. These solvents are formed by adding chemical functional groups to conventional solvents in order to modify their structure. The structure modification refers to changes in the position and size of active regions and changes in the length and strength of ionic bonds. There is another type of amines called "sterically hindered amines" that own weaker CO2-amine bonds; hence lower energy is needed to break their bonds. 2-amino-2-methyl-1-propanol (AMP) and 2-piperidineethanol (PE) are sterically hindered amines [12].

The third generation is amine mixtures method which is meant to combine appropriate features of each category of the aforementioned amines. Adding a solvent with weak performance like tertiary amine to one with strong performance like primary amine leads to forming a blend mixture of solvents that have more extraordinary features than each component as a single solvent. This process is called solvent promotion. MDEA was the first amine to be mixed with amines with faster kinetics to increase the absorption rate [13]. MEA, piperazine (PZ), and DEA are usually used to promote the performance of MDEA. For instance, the absorption rate of PZ is two times greater than that of MEA because PZ has two amine groups in its molecule. That is why PZ is used as a promoter for aqueous MEA solutions [14].

In 2020 Asadi et al. added physical absorbent sulfolane to 2-((2-Aminoethyl) amino) ethanol (AEEA) to form an aqueous solution with different compositions. They conducted an experiment at temperatures of 313.15, 328.15, and 343.15 K and found that this mixture has better performance than MDEA+AEEA. They produced a set of 179 experimental data that is used in this paper. The data set is shown in Table B1 and Table B2 in Appendix B [15].

Response Surface Methodology (RSM) is an approach used in previous works to model and optimize CO2 absorption in different absorbents/adsorbents via various processes. This method is considered a statistical tool in order to reduce the number of experimental tests [16]. RSM modeling results in a polynomial equation whose coefficients describe the importance of each independent variable [17].

Another useful method is Artificial Neural Network (ANN). While existing thermodynamic models suffer low precision, neural networks are well suited for predicting the performance of non-linear and complex systems; hence, in the current study, two algorithms named Radial Basis Function (RBF) and Multi-Layer Perceptron (MLP) were developed by coding in MATLAB and applied to model and simulate CO2 loading in the sulfolane+AEEA mixture using a set of 179 experimental data of the abovementioned work for the first time. These two artificial neural networks are based on learning by trial and error, imitating human learning. Some papers reviewed to create these networks are summarized in Table 1. The ones which used the ANN method have all achieved R2 and MSE values close to 1 and zero, respectively.

Table 1. The list of reviewed articles utilizing different modeling methods (ANN, RSM, and Thermodynamic)

Performance	Approach	Description	Ref.
R^2 = 0.996 (ANN) R^2 = 0.987 (RSM)	ANN, RSM	Modeling of hold up, slip, and characteristic velocities in standard systems using pulsed disc-and-doughnut contactor column	[18]
MSE = 0.0023 (ANN) R^2 = 0.991 (ANN) R^2 = 0.998 (RSM)	ANN, RSM	Hydrodynamic behavior of standard liquid-liquid systems in Oldshue–Rushton extraction column	[19]
R^2 > 0.99 (MLP & RBF)	ANN	Development of Predictive Models for Activated Carbon synthesis from different biomass for CO_2 adsorption using Artificial Neural Networks	[20]
MSE = 0.00004 (MLP) MSE = 0.00071 (RBF)	ANN	Deep learning analysis of Ar, Xe, Kr, and O_2 adsorption on Activated Carbon and Zeolites using ANN approach	[21]
R^2 = 0.944	RSM	Experimental Modeling and Optimization of CO_2 Absorption into Piperazine Solutions Using RSM-CCD Methodology	[17]
AAD% = 15.05	Thermodynamic Modeling	High-pressure measurement and thermodynamic modeling of the carbon dioxide solubility in the aqueous AEEA+ sulfolane system at different temperatures	[15][a]
R^2 = 0.99 (MLP & RBF)	ANN	Prediction of carbon dioxide solubility in ionic liquids using MLP and radial basis function (RBF) neural networks	[22]
AARD% < 10	ANN	Artificial neural network models for the prediction of CO_2 solubility in aqueous amine solutions	[23]
MSE = 0.00023	ANN	Developing a feed forward multilayer neural network model for prediction of CO_2 solubility in blended aqueous amine solutions	[24]
R^2 = 0.9977 AARD% = 2.393	ANN	Modeling of CO_2 loading in aqueous solutions of piperazine: Application of an enhanced artificial neural network algorithm	[25]

-	ANN	Application of artificial neural networks for simulation of experimental CO_2 absorption data in a packed column	[26]
MLP: MSE = 0.00001 R^2 = 0.999 AARD% = 0.267 RBF: MSE = 0.000026 R^2 = 0.999 AARD% = 0.146	ANN	Current Study	

[a] Selected paper for modeling and simulation

Theoretical

Neural networks are designed and utilized based on the human brain's learning algorithm. Simply they receive input/output vectors and find the complicated patterns by which the outputs are obtained by trial and error. The human neurological system includes subsystems called "neurons". Neural messages are transferred through interconnections existing among these neurons. That is, in artificial neural networks, this pattern is developed. A set of inputs are given to neurons and processed there; then, the processed data are given to the output layer [18]. This procedure is repeated until the modeling goal is achieved. This goal can be MSE, R^2, %AARD, etc.

For this study, 179 experimental from Asadi et. al experimental study was used for the modelling and simulation (see Appendix B).

Multi-Layer Perceptron (MLP)

As the name suggests, an MLP network comprises one or more layers of perceptrons; so it is necessary to be familiar with the concept of a perceptron. The simplest type of MLP is a single-layer network, including only one perceptron. All inputs (x_i) and outputs (y_i) (i:1,..,n) are connected to this perceptron. Since inputs and outputs may be of different orders of magnitude, it is preferable first to normalize the independent inputs and then unnormalize the outputs after the training procedure. Eq. 1 is used for normalization purposes. Every feature value of inputs gets multiplied by its corresponding weight value (w_i) and gives ($x_i w_i$) which will be added together further. Finally, the output (y) is obtained by applying the transfer or activation function (f) to the summed value (z), where z and y are shown in Eqs. 2 and 3, respectively and b is called bias or threshold [27].

$$x_i^{norm} = \frac{1-(-1)}{x_{max}-x_{min}} \times x_i + \frac{x_{max} \times (-1) - 1 \times x_{min}}{x_{max}-x_{min}} \quad (1)$$

$$Z = \sum_{i=1}^{n} x_i w_i \quad (2)$$

$$y = f(z) \quad (3)$$

$$Y = \frac{1}{1+e^{-x}} \quad (4)$$

$$Y = \frac{1-e^{-x}}{1+e^{-x}} \quad (5)$$

The processing step within neurons is done using transfer functions such as hardlim[†] or Heaviside, tansig[‡], logsig[§], linear or purelin, etc. [28]. Logsig and tansig functions are demonstrated in Eqs. 4 and 5. linear transfer functions are commonly used in the final layer of a multi-layer network, whereas the logarithmic sigmoid and hyperbolic tangent sigmoid activation functions are typically used in the MLP network's hidden layers [29]. ANNs are highly capable of modeling nonlinear systems by using nonlinear transfer functions and, after that, changing and adjusting neural network parameters like weights (w) and biases (b) during the training process [25].

Only linear transfer functions could be applied to single perceptrons. Eq. 1 is, in fact, the dot product of weight and input vectors. Eq. 1 gives a line that classifies the data into two categories, so if the answer is larger than bias, it gives 1, and if smaller, zero. By adding to the number of perceptrons and layers, MLP is created to deal with nonlinear problems. The first layer is called the input layer, which connects to the first hidden layer. The processed data exiting the first hidden layer go to the second hidden layer, and so on. Outputs of the last hidden layer connect to the last layer, called the output layer. These numbers all flow from the input to the output through hidden layers. This kind of calculation procedure is called feedforward [27].

Since the given outputs are already known, the outputs of the network will be compared to them in order to find the error and deviation of the model [27]. The most common tool is MSE[**] which is presented in Eq. 5 where y_i^{exp}, y_i^{net} and N are given and estimated outputs and number of given data respectively [30]. Eqs. 6 and 7 are the correlation coefficient [18] and average absolute relative deviation [25], respectively.

$$MSE = \frac{1}{N}\sum_{i=1}^{n}(y_i^{exp}-y_i^{net})^2 \quad (5)$$

$$R^2 = \frac{\sum_{i=1}^{n}(y_i^{net}-y_i^{exp})^2}{\sum_{i=1}^{n}(y_i^{net}-y_i^{ave})^2} \quad (6)$$

$$\%AARD = 100 \times \frac{1}{N}\sum_{i=1}^{N}\frac{\left|\alpha_{CO_2,i}^{exp} - \alpha_{CO_2,i}^{net}\right|}{\alpha_{CO_2,i}^{exp}} \quad (7)$$

After one iteration, the back-propagation method is used to modify weights and biases for the new round of calculations. We have tried three algorithms: Levenberg-Marquardt (trainlm), Bayesian Regularization (trainbr), and Scaled Conjugate Gradient (trainscg), among which the Levenberg-Marquardt algorithm was selected for the network. Fig. 1 is the schematic of the developed MLP.

Radial Basis Function Network

A radial basis function (RBF) is a term that refers to any real-valued function whose output is dependent exclusively on the distance of its input from some origin [31]. RBF networks, which

[†] hard-limiter
[‡] Hyperbolic tangent sigmoid
[§] Logarithmic sigmoid
[**] Mean Squared Error

are a type of feedforward neural network, use a supervisory training method to model a data set [22].

RBF and MLP networks use different categorization methods. In MLP networks, hypersurfaces separate the clusters, whereas, in RBF networks, hyperspheres do the same [32]. The general formula for RBF network performance can be written as if the Gaussian function (Euclidean norm) is used as the basis function. The Gaussian function can be mathematically expressed as in Eq. 8 [21]:

$$G(\|x-c_i\| \times b) = exp(-\frac{1}{2\sigma_i^2}(\|x-c_i\| \times b)^2),\ i=1, 2..., N \quad (8)$$

where σ, c_i, x, G, b, and N are variance or spread, centre point, input, output, bias, and the number of the basis function which are cantered at c_i, respectively.

Sums of radial basis functions are typically used to approximate given functions. This approximation process can also be interpreted as a simple kind of neural network; this was the context in which they were originally applied to machine learning [33].

As in the MLP network, MSE and R^2 were the main goals to achieve with respect to gaining the smallest possible number of neurons. A trial-and-error technique was again used to determine this number and change the variance. The developed RBF is depicted schematically in Fig. 2.

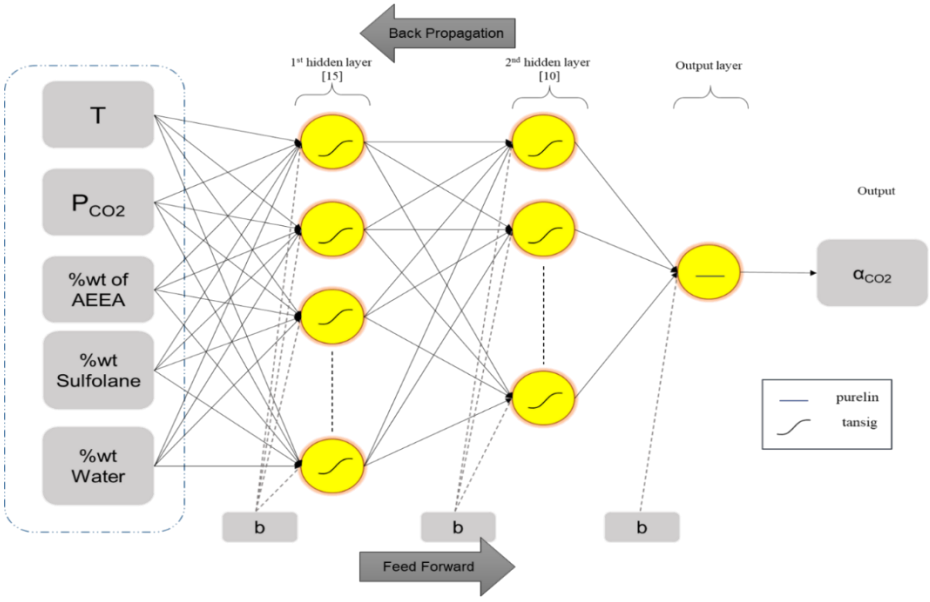

Fig. 1. Schematic of the MLP Network

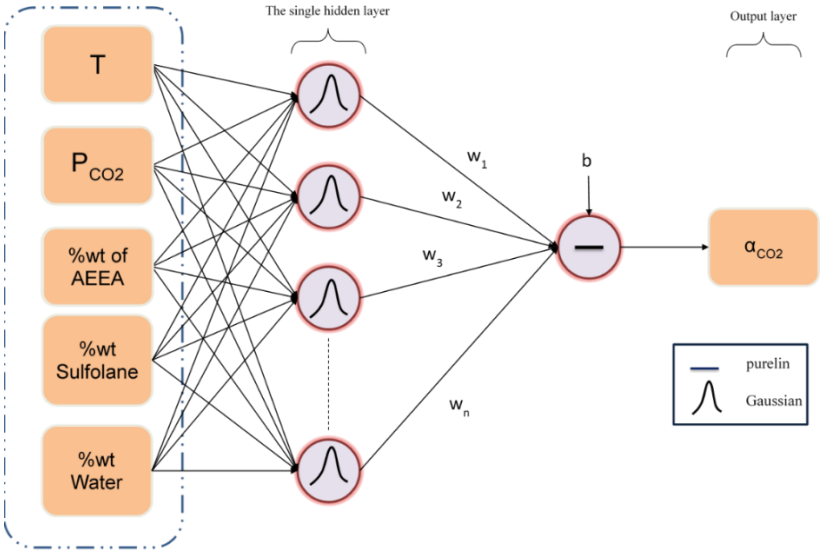

Fig. 2. Schematic of the RBF Network

Results and Discussion

As stated above, two different methods were used to develop a suitable neural network; MLP and RBF. These two networks were capable of training the given data and reaching the goal, which we tend to be the Mean Squared Error (MSE). That is, 179 experimental of the latest Assadi et al. study was used. The structure and results of the aforementioned neural networks will be discussed here.

Multi-Layer Perceptron (MLP)

Various cases were examined by trial and error, from which only some examples are outlined in Table 2. The selected network has 2 hidden layers with 15 and 10 neurons within each, respectively.

Table 2. Examined MLP Networks

Examined MLP Architectures				Statistics				
Run	N_1*	N_2	N_3	Training Function	MSE	%AARD	R^2	Epochs
1	15	12	0	trainbr	6.34E-05	0.2217	0.99984	1778
2	10	10	0	trainbr	1.57E-06	0.1996	0.99986	1058
3	15	12	8	trainbr	7.58E-09	0.2101	0.99981	5288
4	15	12	0	trainscg	1.53E-01	1.2035	0.88626	11
5	15	10	0	trainscg	0.0066	5.9782	0.99365	55
6	15	12	8	trainscg	3.22E-02	5.879	0.97931	21
7	12	10	0	trainlm	9.59E-05	0.7780	0.99800	12
8	15	12	0	trainlm	2.00E-05	0.8243	0.99973	28
9	15	10	0	trainlm	1.22E-05	0.2671	0.99963	42
10	15	12	8	trainlm	2.45E-05	0.2765	0.99975	22

* N_1, N_2, and N_3 are numbers of neurons in each hidden layer, respectively.

The temperature, partial pressure of CO2, and wt.% concentration of mixture components were selected as inputs to the network (5 inputs) and the CO2 loading as output. %80, %5, and 15% of the data were taken for training, validation, and testing, respectively. As it is seen, the ninth

structure has had the best performance. Our goal was to reach the minimum MSE achievable with slight attention to the R2 factor and %AARD.

In order to train the network, we used several back-propagation training algorithms such as 'trainlm', 'trainbr' and 'trainscg', among which the first algorithm performed better than the others. According to Table 2 the Bayesian Regularization learning algorithm is the most accurate but highly time-consuming and takes too many iterations (epochs), hence not appropriate for our work. One important aspect of the training process is the determination of activation functions. For this matter, the first and second hidden layers are given the tangent sigmoid (tansig) function, and the output layer is given pure linear function (purelin).

After finding the structure we were looking for, we extracted biases and weights calculated by the selected network. These values are reported in Table A1 and Table A2, respectively. For the MLP network, the performance and regression diagrams are shown in Fig. 3 and Fig. 4, respectively. According to Fig. 3, the training procedure has stopped when the lowest MSE is achieved. The regression factor of all three steps of modeling in the optimum structure is close to 1, so the processed data are well-fitted. The regression factor of data selected for training, test, and validation, along with that of the overall data, is shown in Fig. 4. All steps of training are well-fitted. Fig. 5 is also a 3-D demonstration of how partial pressure of CO2 and wt.% of AEEA affect CO2 loading at three fixed temperatures (313.15 K, 328.15 K, and 343.15 K). As it is seen, the CO2 loading in the mixture increases by increasing the partial pressure of CO2. Also, the temperature has a direct effect on CO2 loading.

Fig. 6 shows that at a fixed temperature, the aqueous part of the mixture has more contribution to increasing CO2 absorption. By increasing temperature at fixed concentrations of the components, the CO2 loading increases as well.

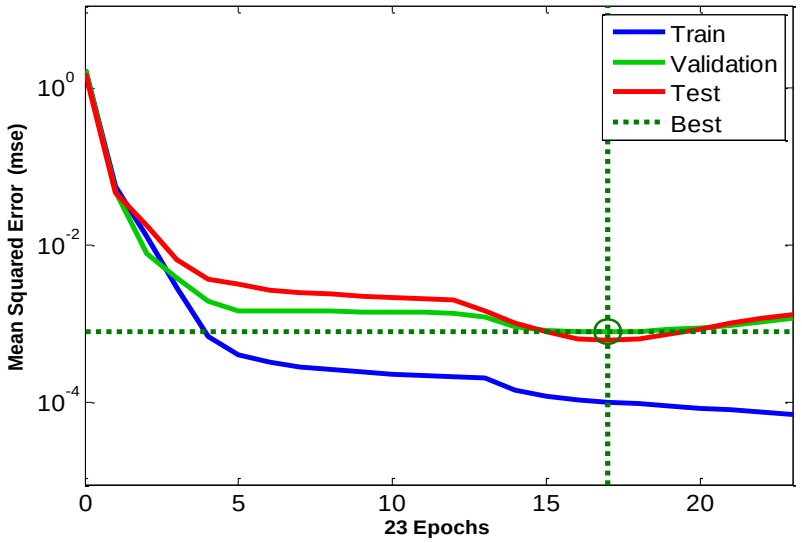

Fig. 3. Performance of the selected MLP network

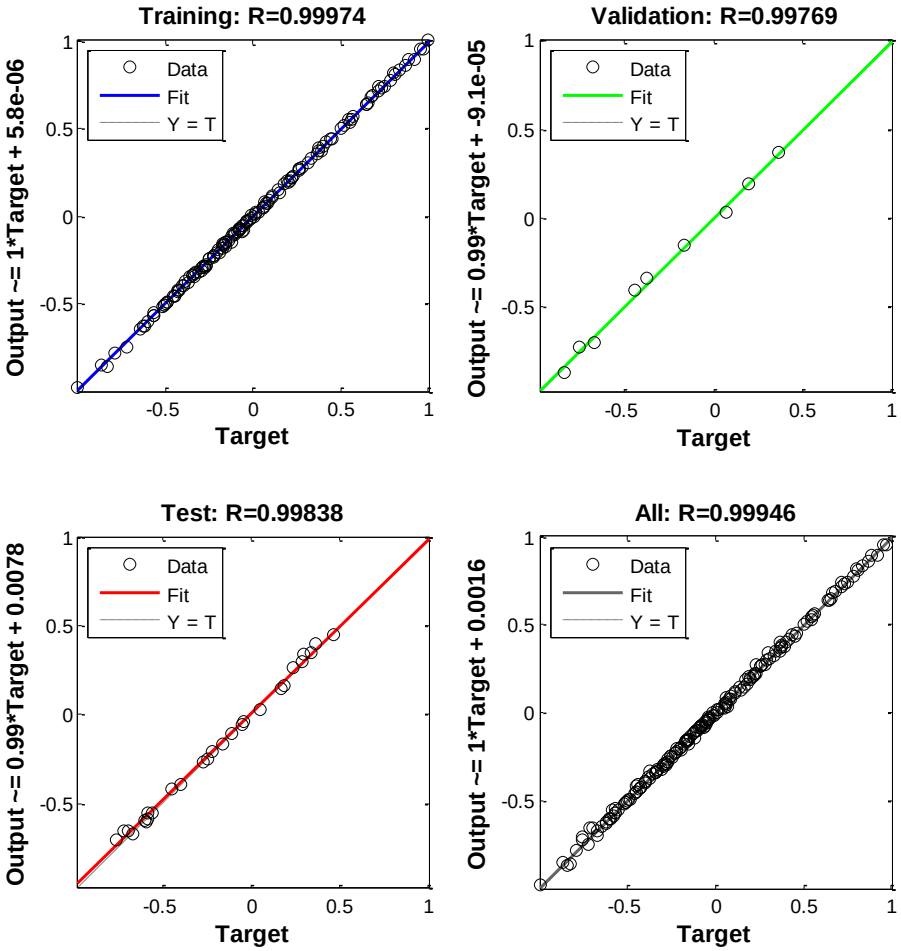

Fig. 4. Regression diagrams of the selected MLP network

In general, increasing the temperature has a reverse effect on CO2 loading. At a fixed temperature, with increasing the partial pressure of CO2, the CO2 loading is significantly increased. In case the aqueous portion of the solution is larger than the AEEA+sulfolane portion, larger values of αCO2 could be obtained.

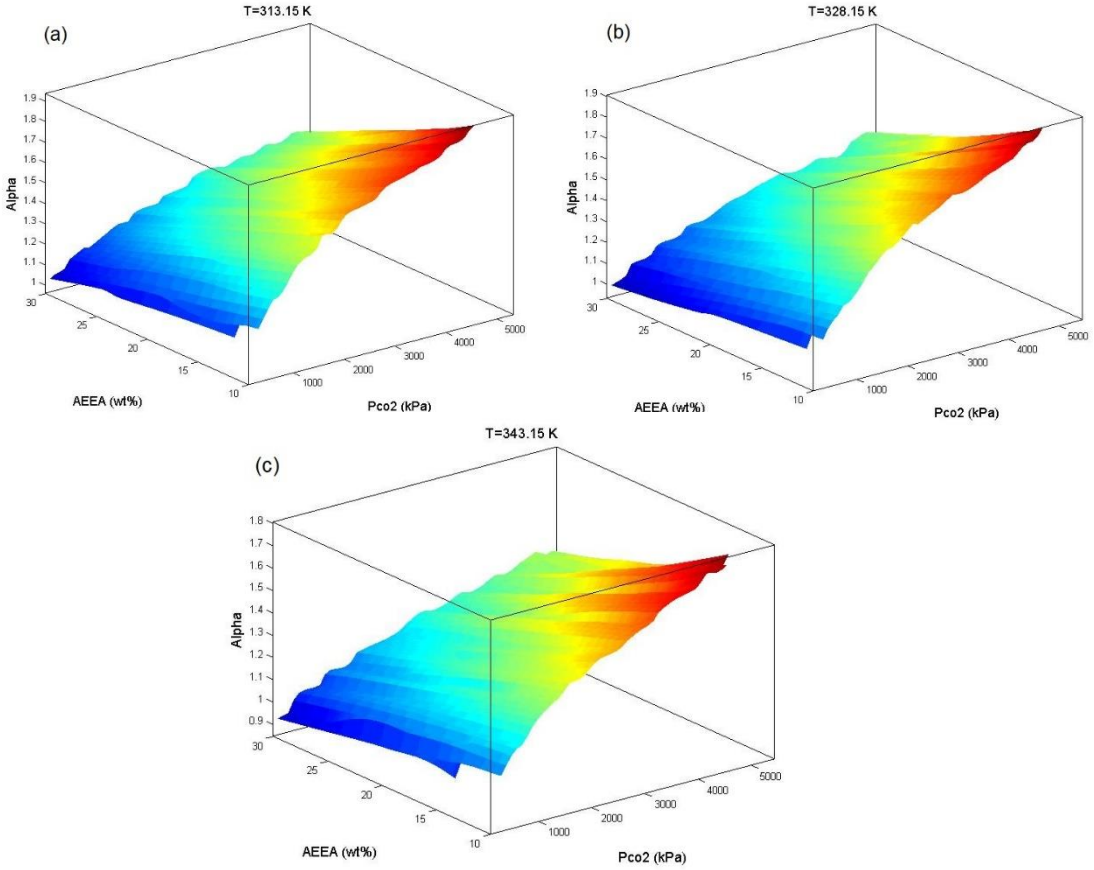

Fig. 5. 3-D demonstration of the effect of pressure, AEEA (wt.%) and temperature on CO_2 loading at a) 313.15 K, b) 328.15 K, and c) 343.15 K

Radial Basis Function (RBF)

Here again, the very same inputs and output were used. Several cases were examined through trial and error, of which only a few are highlighted in Table 3. First, we started from a low value of the number of neurons and variance (spread). The goal was to reach the minimum MSE. As mentioned above, by trial and error, we found out that the best structure to achieve our goal was a network with 138 neurons and a spread value of 2.2. other influential factors were R^2, time, and %AARD, of which the highlighted network had the optimal performance.

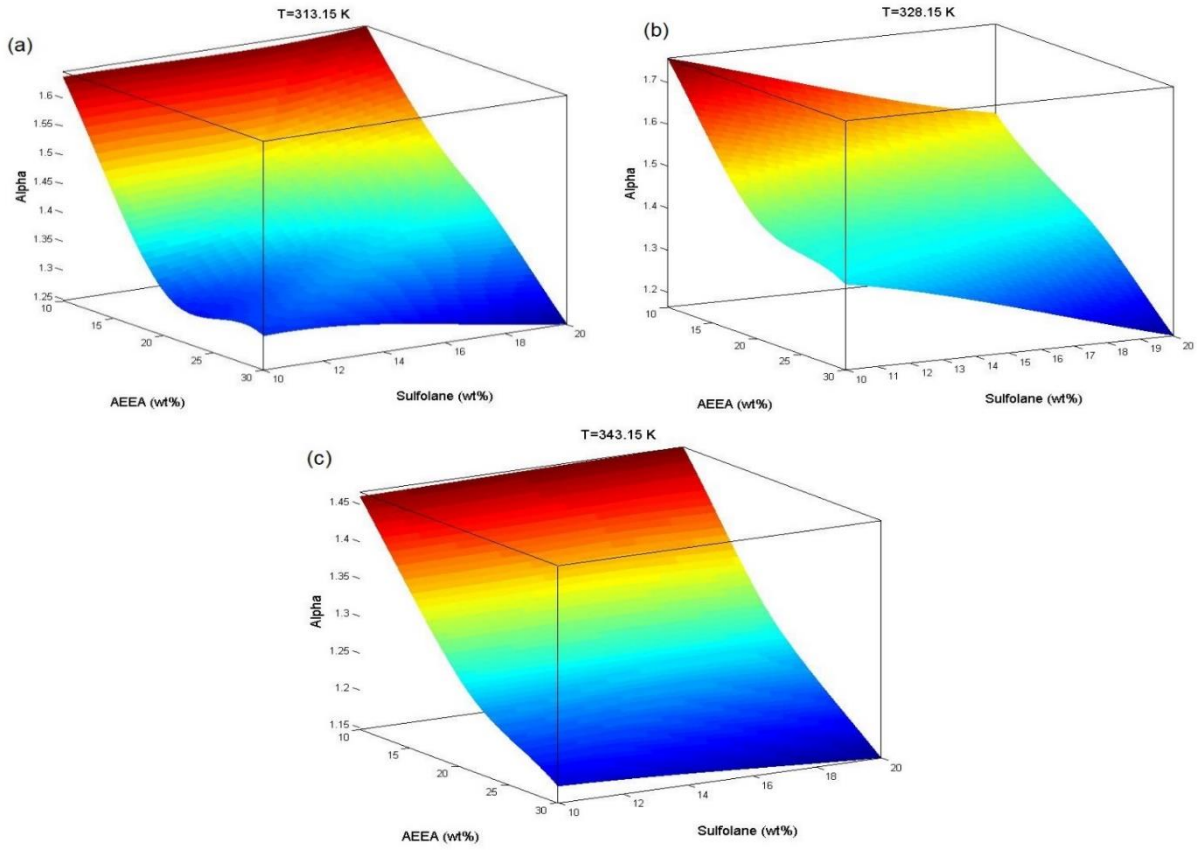

Fig. 6. 3-D demonstration of the effect of AEEA (wt.%), Sulfolane (wt.%) and temperature on CO_2 loading at a) 313.15 K, b) 328.15 K, and c) 343.15 K

Table 3. Examined RBF Networks

Examined RBF Networks			Statistics			
Run	Spread	Neurons	MSE	R^2	t	%AARD
1	2	129	4.25E-05	0.99990	12.10	0.2043
2	2	120	4.53E-05	0.99988	10.37	0.2058
3	2	108	5.10E-05	0.99987	9.41	0.2197
4	2	99	5.37E-05	0.99986	8.59	0.2224
5	2	150	2.83E-05	0.99993	12.47	0.1520
6	2	138	3.62E-05	0.99991	11.43	0.1837
7	2.1	138	2.86E-05	0.99993	11.84	0.1611
8	2.2	138	2.53E-05	0.99993	11.40	0.1460
9	1.9	138	2.14E-05	0.99994	17.86	0.1517
10	1.9	120	3.12E-05	0.99990	10.74	0.1944
11	1.9	150	1.86E-05	0.99995	13.04	0.1302

The regression and performance diagrams for the RBF network are shown in Fig. 6 and Fig. 7, respectively.

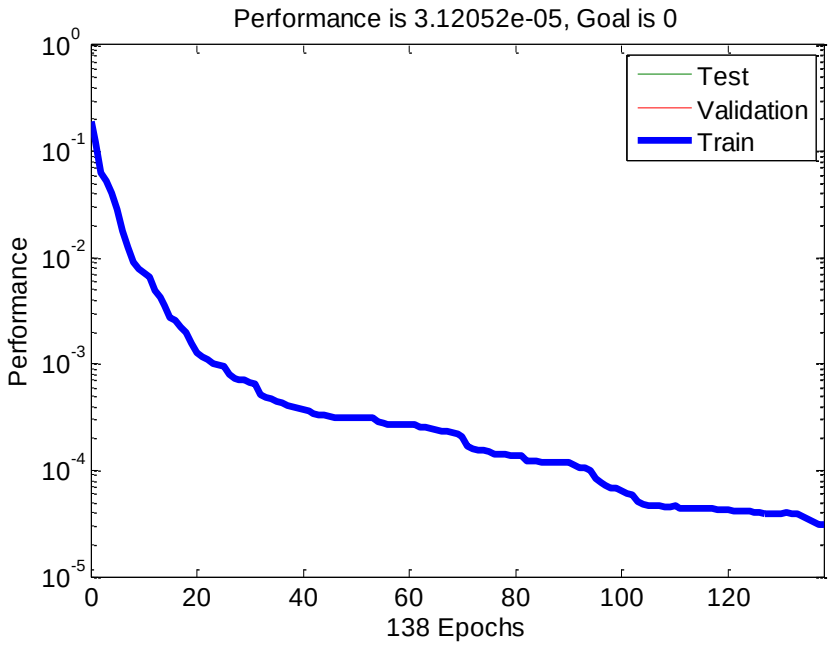

Fig. 7. Performance of the selected RBF network

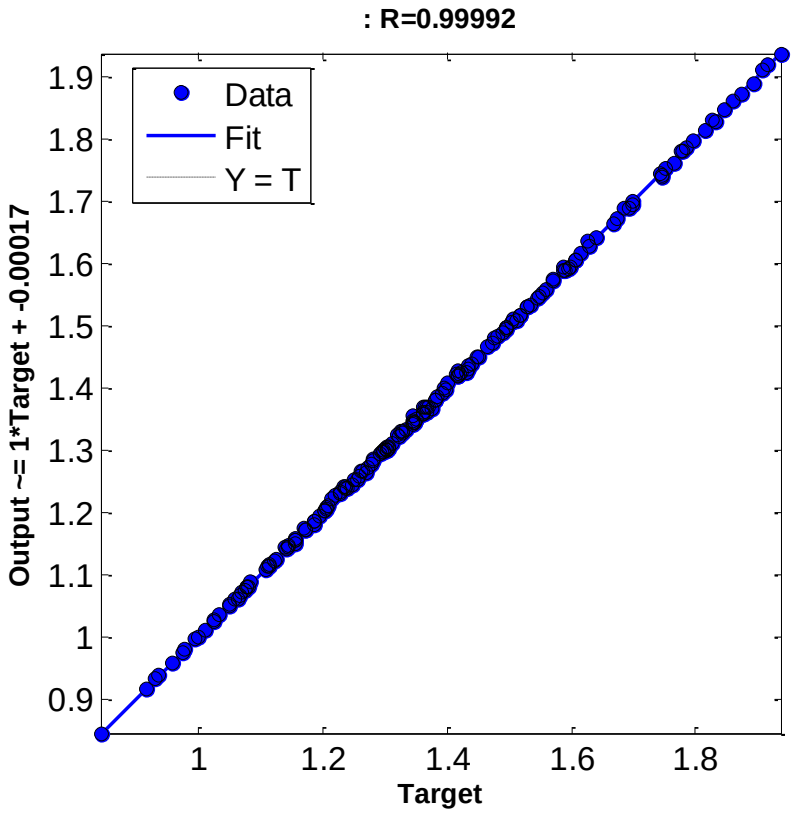

Fig. 8. Regression diagram of the selected RBF Network

Conclusion

In the present work, the CO_2 absorption in a mixture solvent of AEEA+sulfolane was modeled and simulated via Artificial Neural Network (ANN) using MATLAB. The 179 data were obtained from recent research of Assadi et al. Partial pressure of carbon dioxide, temperature and wt.% concentration of AEEA, sulfolane, and water were the five inputs to the system, and CO_2 loading (α_{CO2}) was the only output. Multi-Layer Perceptron (MLP) and Radial Basis Function (RBF) networks were developed to get the minimum MSE (1.22E-05) and maximum R^2 (> 99%) factor possible. The MLP reached our goal by a two-layered network, each containing 15 and 10 neurons, respectively. The RBF network also had a phenomenal performance in achieving the minimum possible MSE (2.53E-05) and maximum R^2 (> 99%) with 138 neurons and a variance value of 2.2. Both optimal networks were acquired by a trial-and-error procedure changing the number of hidden layers and neurons and variance in the MLP and RBF networks, respectively. Also, by calculating the average absolute relative deviation (%AARD), both systems are highly accurate in predicting the experimental data. Finally, more training datasets could be added to the existing models to cover a wider range of input parameters, which can be a field of focus in future studies.

References

[1] Zhang K, Wu J, Yoo H, Lee Y. Machine Learning-based approach for Tailor-Made design of ionic Liquids: Application to CO2 capture. Separation and Purification Technology. https://doi.org/https://doi.org/10.1016/j.seppur.2021.119117

[2] Dashti A, Amirkhani F, Hamedi A-S, Mohammadi AH. Evaluation of CO2 Absorption by Amino Acid Salt Aqueous Solution Using Hybrid Soft Computing Methods. ACS Omega. 2021;6(19):12459-69. https://doi.org/10.1021/acsomega.0c06158

[3] Jiang L, Gonzalez-Diaz A, Ling-Chin J, Roskilly AP, Smallbone AJ. Post-combustion CO2 capture from a natural gas combined cycle power plant using activated carbon adsorption. Applied Energy. 2019;245:1-15. https://doi.org/https://doi.org/10.1016/j.apenergy.2019.04.006

[4] Monjezi AH, Mesbah M, Rezakazemi M, Younas M. Prediction bubble point pressure for CO 2/CH 4 gas mixtures in ionic liquids using intelligent approaches. Emergent Materials. 2021;4(2):565-78.

[5] Yu B, Yu H, Yang Q, Li K, Ji L, Zhang R, et al. Postcombustion Capture of CO2 by Diamines Containing One Primary and One Tertiary Amino Group: Reaction Rate and Mechanism. Energy & Fuels. 2019;33(8):7500-8.

[6] Usubharatana P, Tontiwachwuthikul P. Enhancement factor and kinetics of CO2 capture by MEA-methanol hybrid solvents. Energy Procedia. 2009;1(1):95-102. https://doi.org/https://doi.org/10.1016/j.egypro.2009.01.015

[7] Vaidya PD, Mahajani VV. Kinetics of the reaction of CO2 with aqueous formulated solution containing monoethanolamine, N-methyl-2-pyrrolidone, and diethylene glycol. Industrial & engineering chemistry research. 2005;44(6):1868-73.

[8] Muchan P, Saiwan C, Narku-Tetteh J, Idem R, Supap T, Tontiwachwuthikul P. Screening tests of aqueous alkanolamine solutions based on primary, secondary, and tertiary structure for blended aqueous amine solution selection in post combustion CO2 capture. Chemical Engineering Science. 2017;170:574-82.

[9] Arthur L Kohl RN. Gas Purification. 5th ed: Elsevier; 1997.

[10] Conway W, Bruggink S, Beyad Y, Luo W, Melián-Cabrera I, Puxty G, et al. CO2 absorption into aqueous amine blended solutions containing monoethanolamine (MEA), N,N-dimethylethanolamine (DMEA), N,N-diethylethanolamine (DEEA) and 2-amino-2-methyl-1-propanol (AMP) for post-combustion capture processes. Chemical Engineering Science. 2015;126:446-54. https://doi.org/https://doi.org/10.1016/j.ces.2014.12.053

[11] Liu S, Gao H, He C, Liang Z. Experimental evaluation of highly efficient primary and secondary amines with lower energy by a novel method for post-combustion CO2 capture. Applied Energy. 2019;233-234:443-52. https://doi.org/https://doi.org/10.1016/j.apenergy.2018.10.031

[12] Nematollahi MH, Carvalho PJ. Green solvents for CO2 capture. Current Opinion in Green and Sustainable Chemistry. 2019;18:25-30. https://doi.org/https://doi.org/10.1016/j.cogsc.2018.11.012

[13] Zhao B, Liu F, Cui Z, Liu C, Yue H, Tang S, et al. Enhancing the energetic efficiency of MDEA/PZ-based CO2 capture technology for a 650MW power plant: Process improvement. Applied Energy. 2017;185:362-75. https://doi.org/https://doi.org/10.1016/j.apenergy.2016.11.009

[14] Freeman BC, Bhown AS. Assessment of the technology readiness of post-combustion CO2 capture technologies. Energy Procedia. 2011;4:1791-6. https://doi.org/https://doi.org/10.1016/j.egypro.2011.02.055

[15] Asadi E, Haghtalab A, Shirazizadeh HA. High-pressure measurement and thermodynamic modeling of the carbon dioxide solubility in the aqueous 2-((2-aminoethyl)-amino)-ethanol + sulfolane system at different temperatures. Journal of Molecular Liquids. 2020;314:113650. https://doi.org/https://doi.org/10.1016/j.molliq.2020.113650

[16] Mäkelä M. Experimental design and response surface methodology in energy applications: A tutorial review. Energy Conversion and Management. 2017;151:630-40. https://doi.org/https://doi.org/10.1016/j.enconman.2017.09.021

[17] Pashaei H, Ghaemi A, Nasiri M, Karami B. Experimental Modeling and Optimization of CO2 Absorption into Piperazine Solutions Using RSM-CCD Methodology. ACS Omega. 2020;5(15):8432-48. https://doi.org/10.1021/acsomega.9b03363

[18] Hemmati A, Ghaemi A, Asadollahzadeh M. RSM and ANN modeling of hold up, slip, and characteristic velocities in standard systems using pulsed disc-and-doughnut contactor column. Separation Science and Technology. 2021;56(16):2734-49. https://doi.org/10.1080/01496395.2020.1842890

[19] Ghaemi A, Hemmati A, Asadollahzadeh M, Molaee M. Hydrodynamic behavior of standard liquid-liquid systems in Oldshue–Rushton extraction column; RSM and ANN modeling. Chemical Engineering and Processing - Process Intensification. 2021;168:108559. https://doi.org/https://doi.org/10.1016/j.cep.2021.108559

[20] Mashhadimoslem H, Vafaeinia M, Safarzadeh M, Ghaemi A, Fathalian F, Maleki A. Development of Predictive Models for Activated Carbon Synthesis from Different Biomass for CO2 Adsorption Using Artificial Neural Networks. Industrial & Engineering Chemistry Research. 2021.

[21] Kolbadinejad S, Mashhadimoslem H, Ghaemi A, Bastos-Neto M. Deep learning analysis of Ar, Xe, Kr, and O2 adsorption on Activated Carbon and Zeolites using ANN approach. Chemical Engineering and Processing-Process Intensification. 2021:108662.

[22] Tatar A, Naseri S, Bahadori M, Hezave AZ, Kashiwao T, Bahadori A, et al. Prediction of carbon dioxide solubility in ionic liquids using MLP and radial basis function (RBF) neural networks. Journal of the Taiwan Institute of Chemical Engineers. 2016;60:151-64. https://doi.org/https://doi.org/10.1016/j.jtice.2015.11.002

[23] Chen G, Luo X, Zhang H, Fu K, Liang Z, Rongwong W, et al. Artificial neural network models for the prediction of CO2 solubility in aqueous amine solutions. International Journal of Greenhouse Gas Control. 2015;39:174-84. https://doi.org/https://doi.org/10.1016/j.ijggc.2015.05.005

[24] Hamzehie ME, Mazinani S, Davardoost F, Mokhtare A, Najibi H, Van der Bruggen B, et al. Developing a feed forward multilayer neural network model for prediction of CO2 solubility in blended aqueous amine solutions. Journal of Natural Gas Science and Engineering. 2014;21:19-25. https://doi.org/https://doi.org/10.1016/j.jngse.2014.07.022

[25] Norouzbahari S, Shahhosseini S, Ghaemi A. Modeling of CO2 loading in aqueous solutions of piperazine: Application of an enhanced artificial neural network algorithm. Journal of Natural Gas Science and Engineering. 2015;24:18-25. https://doi.org/https://doi.org/10.1016/j.jngse.2015.03.011

[26] Shahsavand A, Derakhshan Fard F, Sotoudeh F. Application of artificial neural networks for simulation of experimental CO2 absorption data in a packed column. Journal of Natural Gas Science and Engineering. 2011;3(3):518-29. https://doi.org/https://doi.org/10.1016/j.jngse.2011.05.001

[27] Taud H, Mas JF. Multilayer Perceptron (MLP). In: Camacho Olmedo MT, Paegelow M, Mas J-F, Escobar F, editors. Geomatic Approaches for Modeling Land Change Scenarios. Cham: Springer International Publishing; 2018. p. 451-5. https://doi.org/10.1007/978-3-319-60801-3_27

[28] Hagan MT, Demuth HB, Beale M. Neural network design: PWS Publishing Co.; 1997.

[29] Sodeifian G, Niazi Z. Prediction of CO2 absorption by nanofluids using artificial neural network modeling. International Communications in Heat and Mass Transfer. 2021;123:105193.

[30] Mas J-F, Puig H, Palacio JL, Sosa-López A. Modelling deforestation using GIS and artificial neural networks. Environmental Modelling & Software. 2004;19(5):461-71.

[31] Adhikary PP, Dash CJ. Comparison of deterministic and stochastic methods to predict spatial variation of groundwater depth. Applied Water Science. 2017;7(1):339-48. https://doi.org/10.1007/s13201-014-0249-8

[32] Yu H, Xie T, Paszczynski S, Wilamowski BM. Advantages of radial basis function networks for dynamic system design. IEEE Transactions on Industrial Electronics. 2011;58(12):5438-50. https://doi.org/10.1021/acs.energyfuels.9b00961

[33] Broomhead DS, Lowe D. Radial basis functions, multi-variable functional interpolation and adaptive networks. Royal Signals and Radar Establishment Malvern (United Kingdom); 1988.

How to cite: Hasanzadeh A, Ghaemi A, Shahhosseini S. Neural Network Modeling for Development of High-Pressure Measurement of Carbon Dioxide Solubility in the Aqueous AEEA+Sulfolane. Journal of Chemical and Petroleum Engineering 2023; 57(2): 179-197.

Appendix A: Weights and Biases

Table A1. Weights and biases of the first hidden layer

Neurons	T (K)	P_{CO_2} (kPa)	AEEA (%wt)	sulfolane (%wt)	H2O (%wt)	Bias
1	-0.0908	-1.7140	0.3275	-0.7880	-1.4701	2.3451
2	-0.2827	1.5391	-0.4198	-0.3222	-0.7657	1.8438
3	2.0295	2.2140	0.2948	0.5920	0.1106	-1.2899
4	1.4008	0.0620	-1.1339	1.1947	-0.9393	-1.1974
5	0.0520	-1.8130	0.7474	1.3564	1.1204	1.2973
6	-0.0656	-1.1815	-1.7244	0.8154	-1.2336	0.7138
7	-0.7713	-1.3477	-0.9190	-0.1973	-1.7795	-0.0276
8	1.3195	1.2804	0.1624	1.0077	-0.9340	-0.1247
9	-0.2271	-1.6079	0.8947	-0.6138	-0.6736	-0.2058
10	-0.9896	-1.1729	-1.0868	-0.7685	-0.2819	-0.9105
11	0.5844	-0.7953	1.0124	1.7418	-0.4990	0.8112
12	-0.4654	0.7512	0.8760	1.5086	1.5980	-1.3007
13	-2.4564	1.1700	-0.0222	-0.3173	-0.2956	-0.9959
14	-0.5216	0.9676	-0.3159	1.0335	-2.1073	-1.7379
15	-1.8784	0.1157	-0.0769	0.4221	1.5557	-2.3191

Table A2. Weights and biases of the second hidden layer and the output layer

Second hidden layer	**First hidden layer**																**Output layer**	
	1	2	3	4	5	6	7	8	9	10	11	12	13	14	15	Bias	α_{CO_2}	Bias
1	0.9647	-1.1348	0.9468	0.1199	-0.2760	0.0299	0.2077	-0.5793	-0.0436	-0.2009	0.1157	-0.6480	0.1769	0.0767	-0.3213	-1.4776	-0.7444	0.4572
2	0.0109	-0.4931	0.0376	0.1006	-0.3946	0.4061	0.2255	0.7102	0.6065	-0.4990	-0.1879	-0.3713	0.1694	-0.5256	-0.4086	1.2701	-0.1765	
3	-0.4363	-0.5093	0.0446	0.1616	-0.0955	-0.2788	0.6468	0.3549	-0.1069	0.1033	-0.3665	-0.5025	0.5284	0.0578	0.4766	0.9992	-0.9809	
4	-0.1426	-0.4475	-0.3028	-0.0407	-0.2899	0.5472	0.3515	-0.0231	0.7146	-0.6835	0.3463	-0.3040	-0.6149	0.6517	-0.5638	0.6899	-0.2555	
5	-0.4107	-0.0581	-0.2291	0.7296	0.3574	-0.3405	0.3792	0.0493	-0.4336	-0.2532	0.1632	0.1826	0.9603	-0.3606	0.5391	0.1302	0.4195	
6	0.1203	-0.4409	0.5759	-0.5074	-0.7215	-0.7264	-0.3670	-0.5768	-0.1098	-0.6354	-0.7121	0.5756	0.1722	-0.4809	0.3374	0.0223	0.1656	
7	-0.2920	-0.2903	0.0290	0.8894	0.5536	0.5317	-0.5968	0.3692	-0.0887	-0.3326	0.0164	0.9083	0.1875	0.0169	-0.3115	-0.3010	0.3120	
8	-0.1653	0.3483	0.0869	0.4724	-0.0078	0.0350	0.7519	-0.5307	0.6166	0.4921	-0.7220	-0.3314	0.4390	0.7332	-0.2728	0.8028	0.1515	
9	0.5837	-0.7060	-0.3582	0.4262	0.3123	0.2137	-0.5605	-0.3502	0.2343	0.1489	0.3279	0.2617	0.0946	0.2987	-0.2537	1.3632	-0.4640	
10	-0.6501	0.8807	0.3480	-0.5961	-0.1191	0.6567	0.1309	-0.0076	0.1860	0.0711	-0.3895	-0.0266	0.6783	-0.5109	-0.3642	-1.6322	0.7219	

APPENDIX B: The Selected Data

Table B1. The experimental data used for constructing the ANNs at 313.15 K (Asadi et al., 2020)

P_{CO2} (kPa)	α_{CO2}	P_{CO2} (kPa)	α_{CO2}
T=313.15 K, AEEA+sulfolane+H_2O (30-20-50) wt.%		T=313.15 K, AEEA+sulfolane+H_2O (30-10-60) wt.%	
109	0.9576	136	0.9989
495	1.052	565	1.087
983	1.1237	947	1.1412
1784	1.2027	1473	1.1937
2369	1.2525	1842	1.2326
2913	1.2999	2405	1.2768
3377	1.3547	2945	1.3235
3902	1.3669	3691	1.3437
4445	1.3986	4208	1.3683
4996	1.4235	4809	1.3965
		5321	1.4182
T=313.15 K, AEEA+sulfolane+H_2O (20-20-60) wt.%		T=313.15 K, AEEA+sulfolane+H_2O (20-10-70) wt.%	
230	1.1128	270	1.1579
474	1.1723	594	1.2377
920	1.2672	965	1.3028
1386	1.3407	1342	1.3685
1854	1.4066	1934	1.4384
2338	1.4483	2456	1.4958
2996	1.5089	3025	1.5429
3660	1.5593	3681	1.5745
4634	1.6154	4451	1.589
5197	1.6725	5185	1.6289
T=313.15 K, AEEA+sulfolane+H_2O (10-20-70) wt.%		T=313.15 K, AEEA+sulfolane+H_2O (10-10-80) wt.%	
215	1.1561	283	1.2094
693	1.3449	637	1.3585
1453	1.5307	1098	1.4836
1792	1.5909	1570	1.593
2604	1.6987	2044	1.6637
3394	1.7873	2780	1.7425
4012	1.8615	3423	1.7976
4527	1.9352	3904	1.8266
		4289	1.8727
		4597	1.9191

Table B2. The experimental data used for constructing the ANNs at 328.15 K (Asadi et al., 2020)

P_{CO2} (kPa)	α_{CO2}	P_{CO2} (kPa)	α_{CO2}
T=328.15 K, AEEA+sulfolane+H_2O (30-20-50) wt.%		T=328.15 K, AEEA+sulfolane+H_2O (30-10-60) wt.%	
123	0.9314	137	0.975
570	1.0256	608	1.0612
989	1.0787	1134	1.1208
1626	1.1443	1705	1.1732
2117	1.1849	2624	1.2426
2848	1.2522	3228	1.2843
3525	1.3048	3822	1.296
4261	1.3288	4464	1.3215
4928	1.3698	4896	1.3476
5189	1.3925	5448	1.385
T=328.15 K, AEEA+sulfolane+H_2O (20-20-60) wt.%		T=328.15 K, AEEA+sulfolane+H_2O (20-10-70) wt.%	
237	1.0595	191	1.0716
608	1.144	606	1.1707
986	1.2083	1019	1.2414
1456	1.2716	1518	1.3006
2062	1.3452	2056	1.3614
2680	1.42065	2559	1.4265
3242	1.4798	3298	1.4711
4177	1.5164	3983	1.4934
4770	1.5528	4635	1.5303

5286	1.6065	5168	1.5713
T=328.15 K, AEEA+sulfolane+H_2O (10-20-70) wt.%		T=328.15 K, AEEA+sulfolane+H_2O (10-10-80) wt.%	
226	1.107	501	1.242
548	1.2373	744	1.3111
796	1.3056	1195	1.4235
1094	1.3809	1574	1.5159
1638	1.5095	2095	1.6044
2117	1.5879	2859	1.6895
2557	1.6418	3704	1.7541
3058	1.6881	3997	1.7811
3548	1.7399	4475	1.8464
4244	1.8293	4718	1.8895

Table B3. The experimental data used for constructing the ANNs at 343.15 K (Asadi et al., 2020)

P_{CO2} (kPa)	α_{CO2}	P_{CO2} (kPa)	α_{CO2}
T=343.15 K, AEEA+sulfolane+H_2O (30-20-50) wt.%		T=343.15 K, AEEA+sulfolane+H_2O (30-10-60) wt.%	
84	0.8446	184	0.9168
411	0.9377	512	0.9951
1034	1.0245	1087	1.0665
1551	1.0794	1625	1.1159
2286	1.1497	2562	1.1801
2901	1.2276	2997	1.2207
3611	1.2643	3708	1.2574
4251	1.3001	4452	1.2945
4794	1.3329	5130	1.3273
5086	1.3615	5425	1.3502
T=343.15 K, AEEA+sulfolane+H_2O (20-20-60) wt.%		T=343.15 K, AEEA+sulfolane+H_2O (20-10-70) wt.%	
197	0.9782	174	1.0113
420	1.049	398	1.08
924	1.1451	564	1.1124
1404	1.2026	823	1.1547
2016	1.2658	1418	1.229
2437	1.3015	1965	1.2815
3129	1.3573	2571	1.3311
4097	1.4345	3071	1.3685
4735	1.4655	3849	1.4184
5253	1.5049	4838	1.4505
		5428	1.4895
T=343.15 K, AEEA+sulfolane+H_2O (10-20-70) wt.%		T=343.15 K, AEEA+sulfolane+H_2O (10-10-80) wt.%	
205	1.0361	232	1.0728
673	1.2049	526	1.1861
1423	1.3807	941	1.2956
1752	1.4309	1529	1.4207
2594	1.532	2127	1.4982
3244	1.6373	2650	1.5466
4168	1.7615	3097	1.5938
4631	1.8152	3896	1.694
		4306	1.7456
		4589	1.7796